AGU PUBLICATIONS

JGR

Journal of Geophysical Research: Earth Surface

RESEARCH ARTICLE
10.1002/2014JF003291

Key Points:
- RES-sounded internal layers in Institute/Möller Ice Streams show flow changes
- Ice-flow reconfiguration evinced in Bungenstock Ice Rise to higher tributaries
- Holocene dynamic reconfiguration occurred in much of IIS/MIS as ice thinned

Supporting Information:
- Sections S1–S4 and Figure S1

Correspondence to:
R. G. Bingham,
r.bingham@ed.ac.uk

Citation:
Bingham, R. G., D. M. Rippin, N. B. Karlsson, H. F. J. Corr, F. Ferraccioli, T. A. Jordan, A. M. Le Brocq, K. C. Rose, N. Ross, and M. J. Siegert (2015), Ice-flow structure and ice dynamic changes in the Weddell Sea sector of West Antarctica from radar-imaged internal layering, *J. Geophys. Res. Earth Surf.*, *120*, 655–670, doi:10.1002/2014JF003291.

Received 21 JUL 2014
Accepted 3 FEB 2015
Accepted article online 6 FEB 2015
Published online 3 APR 2015

Ice-flow structure and ice dynamic changes in the Weddell Sea sector of West Antarctica from radar-imaged internal layering

Robert G. Bingham[1], David M. Rippin[2], Nanna B. Karlsson[3], Hugh F. J. Corr[4], Fausto Ferraccioli[4], Tom A. Jordan[4], Anne M. Le Brocq[5], Kathryn C. Rose[6], Neil Ross[7], and Martin J. Siegert[8]

[1]School of GeoSciences, University of Edinburgh, Edinburgh, UK, [2]Environment Department, University of York, York, UK, [3]Centre for Ice and Climate, Niels Bohr Institute, University of Copenhagen, Copenhagen, Denmark, [4]British Antarctic Survey, Natural Environment Research Council, Cambridge, UK, [5]Geography, College of Life and Environmental Sciences, University of Exeter, Exeter, UK, [6]Bristol Glaciology Centre, School of Geographical Sciences, University of Bristol, Bristol, UK, [7]School of Geography, Politics and Sociology, Newcastle University, Newcastle, UK, [8]Grantham Institute and Department of Earth Science and Engineering, Imperial College London, London, UK

Abstract Recent studies have aroused concerns over the potential for ice draining the Weddell Sea sector of West Antarctica to figure more prominently in sea level contributions should buttressing from the Filchner-Ronne Ice Shelf diminish. To improve understanding of how ice stream dynamics there evolved through the Holocene, we interrogate radio echo sounding (RES) data from across the catchments of Institute and Möller Ice Streams (IIS and MIS), focusing especially on the use of internal layering to investigate ice-flow change. As an important component of this work, we investigate the influence that the orientation of the RES acquisition track with respect to ice flow exerts on internal layering and find that this influence is minimal unless a RES flight track parallels ice flow. We also investigate potential changes to internal layering characteristics with depth to search for important temporal transitions in ice-flow regime. Our findings suggest that ice in northern IIS, draining the Ellsworth Subglacial Highlands, has retained its present ice-flow configuration throughout the Holocene. This contrasts with less topographically constrained ice in southern IIS and much of MIS, whose internal layering evinces spatial changes to the configuration of ice flow over the past ~10,000 years. Our findings confirm Siegert et al.'s (2013) inference that fast flow was diverted from Bungenstock Ice Rise during the Late Holocene and suggest that this may have represented just one component of wider regional changes to ice flow occurring across the IIS and MIS catchments as the West Antarctic Ice Sheet has thinned since the Last Glacial Maximum.

1. Introduction

Many ice streams draining the West Antarctic Ice Sheet (WAIS) rest on beds below current sea level that deepen inland, rendering them vulnerable to rapid retreat [e.g., *Schoof*, 2007; *Joughin and Alley*, 2011; *Ross et al.*, 2012; *Favier et al.*, 2014]. Dynamic instability is further evinced by observations that some ice streams experience spatial migration [*Echelmeyer and Harrison*, 1999; *Catania et al.*, 2005], dramatic decelerations or "shutdowns" [*Retzlaff and Bentley*, 1993; *Catania et al.*, 2006], and flow switching or ice stream piracy between neighboring systems [*Jacobel et al.*, 1996; *Conway et al.*, 2002; *Vaughan et al.*, 2008]. These phenomena require improved understanding and representation in next generation ice sheet models as they aim toward better forecasts of ice sheet response to climatic forcing [cf., *Vaughan et al.*, 2013]. An outstanding limitation concerns our observational database of WAIS ice stream histories, which remains relatively sparse both in terms of spatial extent and temporal coverage. Most dynamic phenomena have been observed for ice streams draining either to the Ross Sea, via the Siple Coast and Ross Ice Shelf, or to the Amundsen Sea. By contrast, the dynamics of ice streams draining to the Weddell Sea, via the Filchner-Ronne Ice Shelf (FRIS), remain largely unknown. The primary reason for this has been a dearth of survey data. Ice streams in the Weddell Sea sector (WSS) have not been highlighted as regions of potential major ice loss by satellite altimetry [*Pritchard et al.*, 2009; *McMillan et al.*, 2014]; the conventional assumption being that inland ice is protected from external forcing by the FRIS. However, several recent studies now collectively suggest that the WSS may be far more dynamic than previously thought.

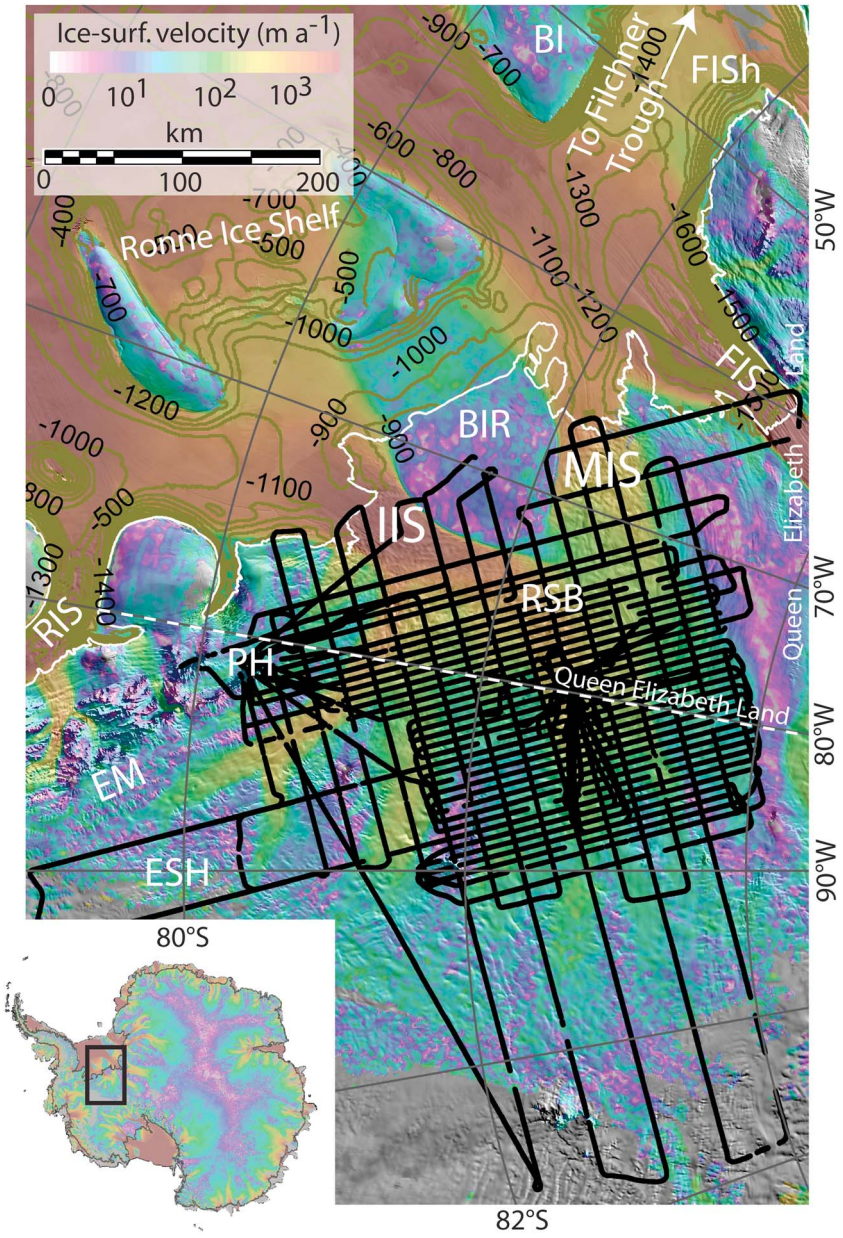

Figure 1. Location and configuration of RES data acquired in 2010/2011 and used in this paper (black lines). The background shows the satellite-derived surface ice-flow velocities from MEaSUREs [*Rignot et al.*, 2011] superimposed over MODIS satellite imagery [*Haran et al.*, 2006]; the white line is the ASAID grounding line [*Bindschadler et al.*, 2011]. The inset depicts location in Antarctica. The elevation of the seafloor below the Filchner-Ronne Ice Shelf is shown as contours derived from Bedmap2 [*Fretwell et al.*, 2013]. BI = Berkner Island, BIR = Bungenstock Ice Rise, EM = Ellsworth Mountain Range, ESH = Ellsworth Subglacial Highlands, FIS = Foundation Ice Stream, FISh = Filchner Ice Shelf, IIS = Institute Ice Stream, MIS = Möller Ice Stream, PH = Patriot Hills, RIS = Rutford Ice Stream, and RSB = Robin Subglacial Basin.

One signal of this potential for change in the WSS is provided by the short-term behavior of the grounding zone and the recent evolution of ice plains there. *Brunt et al.* [2011] used repeat ICESat laser altimetry to show that much of the grounding zone between Institute Ice Stream (IIS; 81.5°S, 75°W), Möller Ice Stream (MIS; 82.5°S, 71°W), and Foundation Ice Stream (83°S, 60°W; Figure 1) includes three ice plains at the point of flotation. Reanalysis of the WSS grounding zones using Lagrangian filtering further reveals thinning concentrated around the FRIS grounding line [*Moholdt et al.*, 2012]. Should these presently grounded zones

thin further and become ungrounded—a feasible prospect should warm oceanwater access the subshelf cavity and induce basal melting—ice dynamics could progressively change inland, as witnessed elsewhere in the WAIS [e.g., *Flament and Rémy*, 2012; *Pritchard et al.*, 2012]. Recent oceanographic modeling by *Hellmer et al.* [2012] supports this possibility, showing that a redirection of the coastal current into the Filchner Trough (Figure 1) and underneath FRIS would lead to increased movement of warm waters into the deep southern ice-shelf cavity. Inland from the WSS grounding line, several investigations reveal an environment in which ice stream dynamism is possible. *Scambos et al.* [2004] inferred from a combination of satellite-acquired optical and radar remote sensing observations that the bed of IIS is composed of weak material, and *Bingham and Siegert* [2007] used reconnaissance radio echo sounding (RES) data from the 1970s to quantify bed roughness and demonstrate that marine sediments were likely distributed widely throughout the lower IIS and MIS catchments. With more comprehensive RES data acquired in 2010/2011, it was recognized that the beds of both IIS and MIS deepen steeply inland to the Robin Subglacial Basin (Figure 1), making them susceptible to ice stream retreat should FRIS buttressing diminish [*Ross et al.*, 2012]. Further inland, several tectonically controlled subbasins are present [*Jordan et al.*, 2013]. Analysis of bed roughness across the catchment suggests that the Robin Subglacial Basin is filled with sediments, likely of marine origin [*Rippin et al.*, 2014], and is similar in characteristics to ice sheet beds reported from elsewhere that are associated with ice sheet change [e.g., *Anandakrishnan et al.*, 1998; *Tulaczyk et al.*, 2000; *Peters et al.*, 2006]. Indeed, *Siegert et al.* [2013] have recently presented evidence that the Bungenstock Ice Rise (BIR; Figure 1) may have transitioned from hosting fast ice flow to its present, slow-flow "ice-rise" state, as recently as 400 to 4000 years ago, requiring significant modifications to the ice flow upstream.

In this paper, we examine the spatial and temporal stability of ice flow across IIS and MIS using aerogeophysical data gathered over the region during the 2010/2011 austral summer season. A particular focus is the analysis of internal layering patterns across the catchments with the objective of extracting from these evidence of past changes in ice flow. Our analyses suggest that inland ice in upstream IIS and across MIS, being relatively unconstrained by topography, has experienced reconfiguration during the Holocene that is expressed by disruption to internal layering patterns.

2. Methods

2.1. Data

The primary data set used in this paper comprises >25,000 line kilometers of RES data acquired as part of an aerogeophysical survey of the IIS and MIS catchments during the austral season 2010/2011 (Figure 1). Data were collected with the British Antarctic Survey Polarimetric-radar Airborne Science INstrument (PASIN); survey specifications are detailed in *Ross et al.* [2012], and further technical details of the instrumentation are given in *Corr et al.* [2007].

We applied 2-D "synthetic aperture radar" (SAR) processing to all the data. SAR processing removes off-nadir reflections and refocuses received energy to its original location. It can also be used to reduce clutter and extraneous hyperbolae often present in areas of rough subglacial topography. Further details of the processing as applied to PASIN acquisition are supplied in *Hélière et al.* [2007] and T. Newman (Application of synthetic aperture techniques to radar echo soundings of the Pine Island Glacier, Antarctica, unpublished PhD thesis, Univ. Coll. London, London, 2011). The use of SAR processing is particularly important when the primary objective is to pick the basal interface for input into digital elevation models [e.g., *Ross et al.*, 2012; *Fretwell et al.*, 2013] and analyses of bed roughness [*Rippin et al.*, 2014]. SAR processing allows precise examination (including tracing) of internal layering as it declutters hyperbolae arising from reflectors that are points directly beneath or near-horizontal linear features perpendicular to the flight track (T. Newman, unpublished PhD thesis, 2011).

RES profiles were generated at a data rate of 13 Hz giving a spatial sampling interval of ~10 m and written to seismic standard SEG-Y format. The bed was picked semiautomatically using PROMAX seismic processing software, and ice thickness was determined using a radio wave travel speed of 0.168 m ns^{-1} offset by a nominal value of 10 m travel at airspeed to correct for the firn layer [*Ross et al.*, 2012]. Error due to this assumption is estimated at ±3 m.

Although we do not have dating control on the ice across IIS/MIS, age-depth modeling at BIR, in the lower catchment, suggests that ice at 40% of ice thickness is ~4000 years old [*Siegert et al.*, 2013], suggesting that the deepest ice in many parts of the catchment extends well beyond the Holocene.

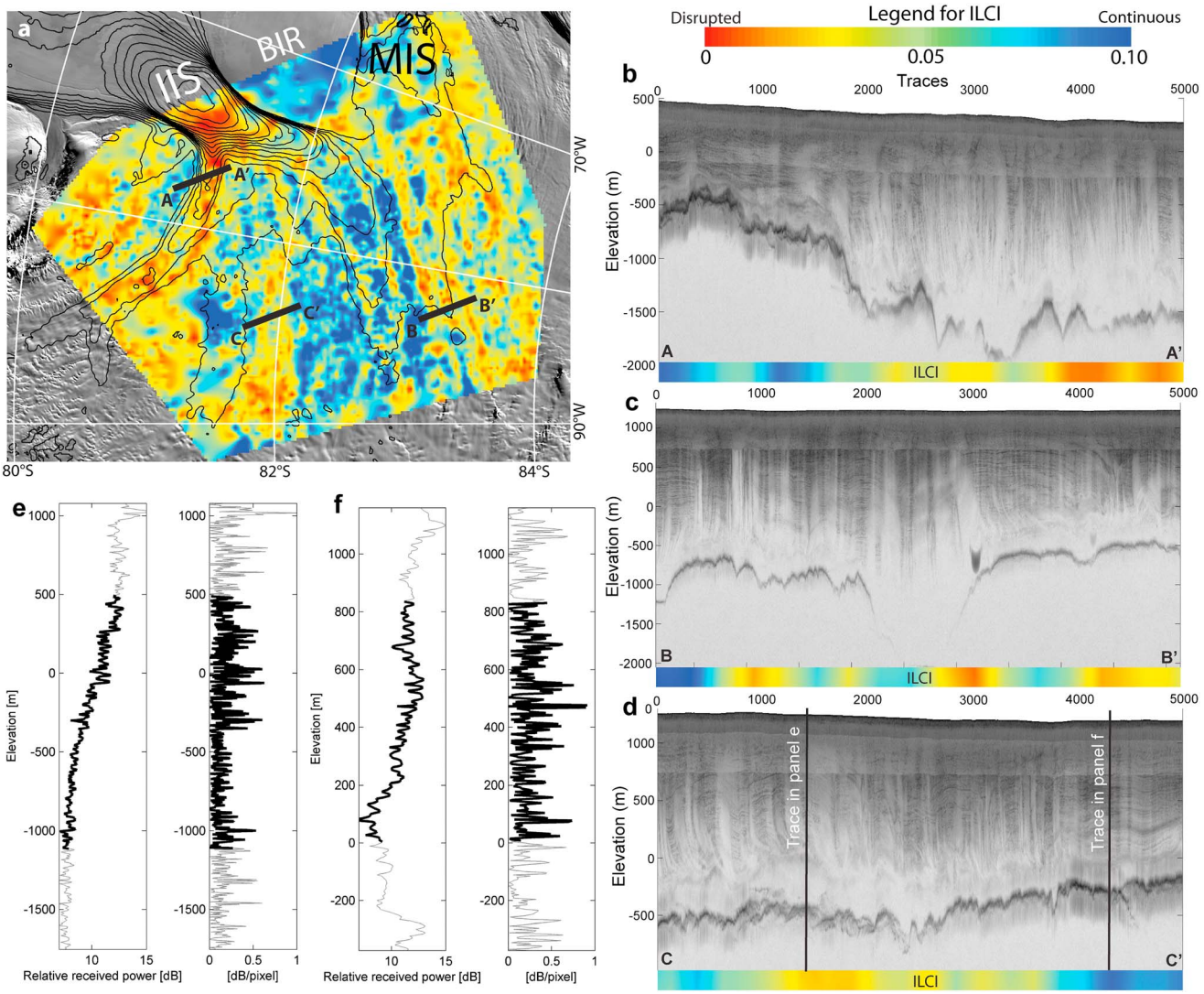

Figure 2. (a) Gross internal layering properties mapped across IIS and MIS. ILCI plotted here is calculated using 100 trace moving windows along RES flight tracks, with the result gridded at 2.5 km^2 resolution using ArcGIS "Topo-to-Raster." The background is from MODIS imagery [*Haran et al.*, 2006], and the black contours mark 25 m a^{-1} surface ice-flow velocities [*Rignot et al.*, 2011]. The same ILCI result, plotted along flight tracks, is given in Figure S1 in the supporting information. (b–d) The color bar gives the ILCI result for the layering behavior that can be viewed qualitatively in the radargrams. Flight tracks AA′, BB′, and CC′, whose 2-D SAR radargrams are depicted in Figures 2b–2d, respectively, are annotated in panel (a). (e) A-scope (left) and absolute value of the gradient of the A-scope (right) for a trace from profile CC′ characterized by disrupted layering. The gray line depicts the whole trace, while overlaid in black is the section used for calculation of ILCI. (f) Same as in Figure 2e but for a trace from profile CC′ characterized by continuous internal layering. Note the generally higher oscillations for this trace through strong layers, which will ultimately contribute toward a higher ILCI indicative of continuous layering.

2.2. Analysis of Internal Layering

Multiple internal (also known as englacial) layers are present in all the RES profiles acquired across IIS and MIS (Figure 2). They represent boundaries in the dielectric properties of the ice, off which a small fraction of the radar signal reflects. Most of these likely arise from paleoaccumulation-derived contrasts in ice acidity [e.g., *Hempel et al.*, 2000] but nearer the surface may reflect density contrasts [e.g., *Moore*, 1988]. Deeper internal layers may result from anisotropic ice crystal fabric [*Siegert and Kwok*, 2000; *Siegert and Fujita*, 2001; *Eisen et al.*, 2007]. Internal layers may not always represent single physical layers in the ice itself: rather, they are radiological interference phenomena which may at different times represent single layers or groups of closely spaced layers and whose specific characteristics will vary according to the radar system being used to detect them. Crucially, none of these considerations rules out the treatment of

internal layers as isochrones; it is this property that makes internal layers vital and often the only records of past ice accumulation and ice-flow histories [e.g., *Jacobel et al.*, 1993; *Siegert and Payne*, 2004; *Waddington et al.*, 2007; *Neumann et al.*, 2008; *MacGregor et al.*, 2009; *Leysinger Vieli et al.*, 2011; *Karlsson et al.*, 2014].

Of especial focus here, internal layers can record information about the locations and flow dynamics both of current and past ice streams and ice stream tributaries. Previous examinations of RES data sets from several regions of Antarctica have demonstrated that in ice streams, and the tributaries that feed them, internal layering becomes disrupted or "buckled" due to increased englacial stress gradients caused by differential and/or convergent flow, and flow around subglacial obstacles [e.g., *Jacobel et al.*, 1993; *Rippin et al.*, 2003; *Siegert et al.*, 2003; *Ng and Conway*, 2004; *Bingham et al.*, 2007; *Hindmarsh et al.*, 2007; *Ross et al.*, 2011]. Recently, *Karlsson et al.* [2012] developed an "Internal Layering Continuity Index" (hereafter ILCI), which is useful in characterizing, with relative rapidity, regions of apparently continuous versus disrupted internal layering from large-volume RES data sets. Here we follow earlier convention [*Rippin et al.*, 2003; *Siegert et al.*, 2003] in using the phrase "disrupted layering" to refer to ice where the layering diverges significantly from the ice bed and/or surface and the term "continuous layering" to refer to ice wherein the layers predominantly follow the surface and bed. Examples of apparently continuous and disrupted layering, associated with their derived ILCI values, are shown in Figure 2. The method is introduced in *Karlsson et al.* [2012], and we provide further details, and advice pertaining to appropriate deployment conditions, in the supporting information of this paper. Our primary use of the ILCI here is to target regions of internal layering disruption from the large data set. These regions can then be studied in more detail, with supplementary evidence such as subglacial topography and contemporary ice-flow patterns, to diagnose possible changes to ice flow across the IIS/MIS catchments.

3. Results and Analysis

3.1. Regional Internal Layering Properties

Figure 2a illustrates a regional view of the gross internal layering properties across IIS and MIS derived using the ILCI method. Specifically, Figure 2a depicts ILCI calculated from 100 trace moving windows (equating to ~1 km or 0.5–1 ice thicknesses), applied to the middle three fifths of the full ice column, and then gridded to 2.5 km^2. The decision to use this combination of moving window size and grid resolution represents the conclusion of sensitivity testing concerning the effects on ILCI of varying these parameters across the IIS/MIS data set and comprises the optimal balance between capturing too much local (in this case subkilometer) detail versus overly smoothing regional trends (see section S1.3 in the supporting information). The application to the middle three fifths of the ice column is based on previous experience discussed in *Karlsson et al.* [2012] and in section S1.1 in the supporting information of this paper. Importantly, these choices need to be made in applying ILCI to any RES data set; hence, both caution and judgment are required when comparing ILCI results between different regions/data sets; see further discussion in the supporting information.

Figure 2a shows spatial coherence in internal layering properties across IIS and MIS. In the main trunk of IIS, and within the dissected terrain draining from the Ellsworth Subglacial Highlands, high ILCI corresponds with slow ice flow and low ILCI with tributary and ice stream (faster) flow. Further inland, in the upstream IIS catchment and across MIS, internal layering (as represented by ILCI) also appears spatially organized, but notably, the patterning in the ILCI does not match the current surface ice-flow configuration. In some previous studies, a mismatch between internal layering properties and contemporary ice dynamics has been taken as evidence for a change in regional ice-flow regime [e.g., *Bingham et al.*, 2007; *Woodward and King*, 2009]. Before being able to reach such a conclusion with confidence, it is necessary to consider possible effects on internal layering imposed by the direction of RES data acquisition (section 3.2) and subglacial topography. The latter objective is achieved by considering the internal layering patterns alongside supplementary data sets (section 4.1).

3.2. Effect of Ice-Flow Direction on Internal Layering Properties

In RES data such as those analyzed here, radargrams containing internal layers represent two-dimensional snapshots of three-dimensional fields, which we expect to be influenced fundamentally by the anisotropic nature

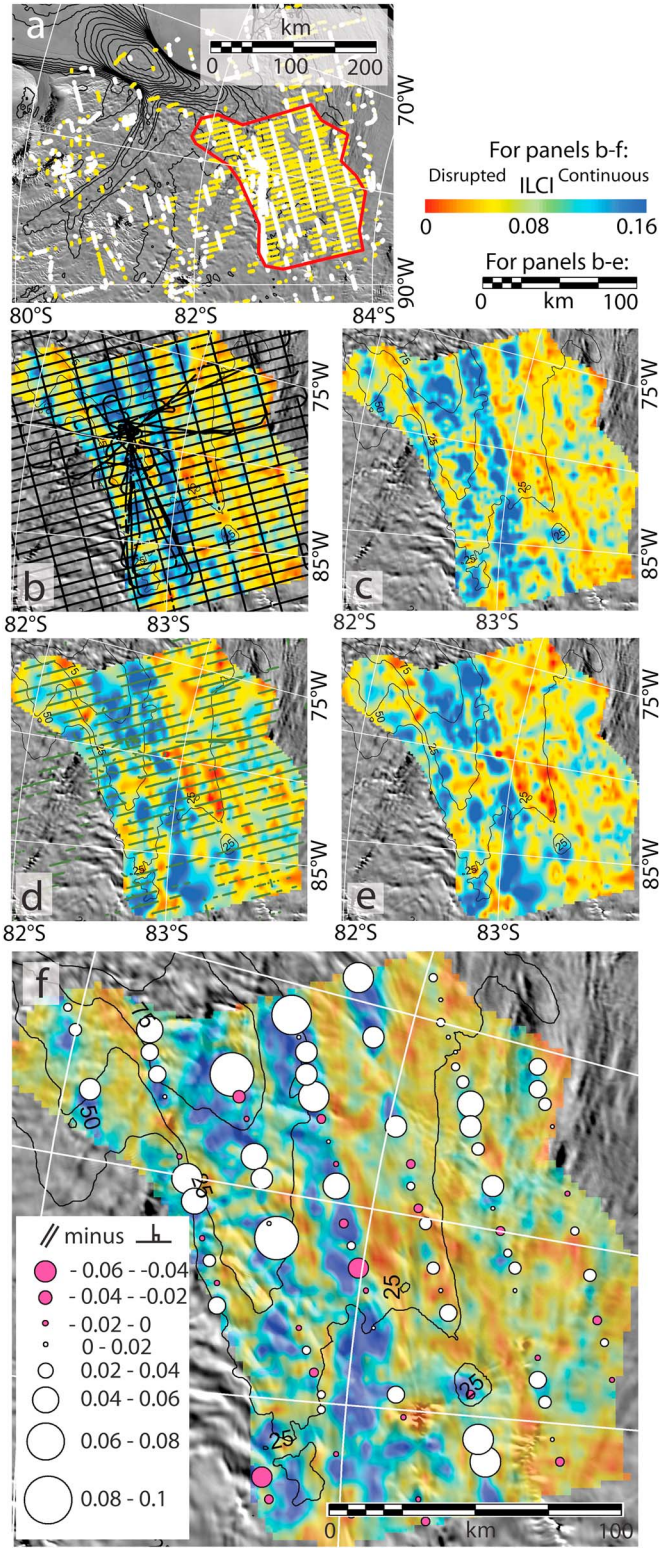

of ice stream flow. There is therefore a cause to expect that the direction of a RES acquisition track relative to the direction of ice flow may influence the properties observed in the RES data, as noted by *Ng and Conway* [2004] and as has been observed both quantitatively and qualitatively in intersecting RES profiles [e.g., *Bingham et al.*, 2007, Figure S1a in the supporting information to this paper]. This possible directional bias has been addressed in recent RES data analyses of ice sheet bed roughness [*Bingham and Siegert*, 2009; *Gudlaugsson et al.*, 2013], including the analysis of bed roughness from the RES survey central to this paper [*Rippin et al.*, 2014]. However, prior to this study, we are unaware of any systematic investigation of the influence of RES acquisition track relative to ice-flow direction having been conducted on internal layering data.

We filtered two subsets of RES data from the original data set—one containing only RES tracks "parallel" to ice flow and the other containing solely tracks "perpendicular" to ice flow. Here parallel is defined as being within 10° of the direction of ice flow and perpendicular to within 10° of normal to the direction of ice flow; ice-flow directions being taken from the National Snow and Ice Data Center MEaSUREs database of satellite-derived ice surface velocities (based on satellite

Figure 3. Analysis of ILCI results relative to ice-flow direction, with background imagery and contours as in Figure 2a. (a) Flight tracks within 10° of being parallel (white) and perpendicular (yellow) to ice flow. The red polygon demarcates region of interest where a high concentration of flight tracks fulfills the above criteria and is hence used for further panels. (b and c) ILCI results for all RES data. Figure 3b shows the flight tracks used to generate the result. (d and e) ILCI results generated only from perpendicular-to-flow RES data. Figure 3d marks the analyzed tracks. (f) Plot of parallel-to-flow ILCI minus perpendicular-to-flow ILCI where orthogonal RES profiles intersect (proportional circles); the background result is repeated from Figure 3c.

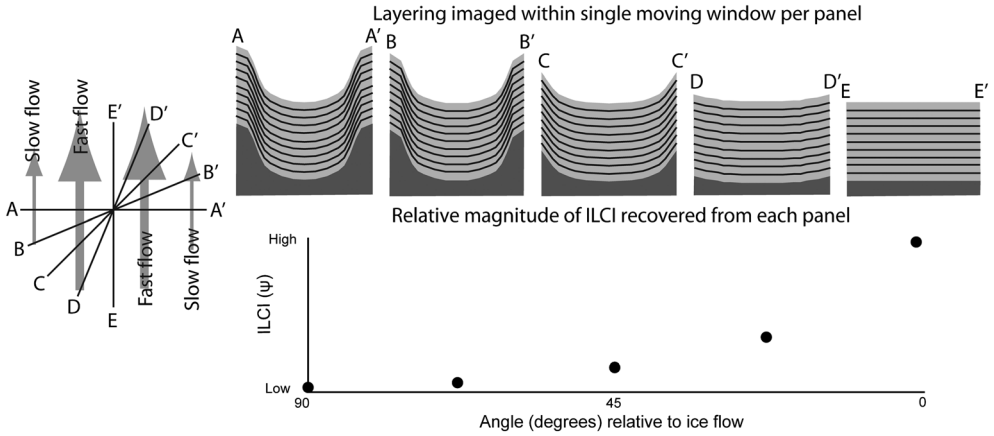

Figure 4. Schematic diagram to demonstrate the influence of ice-flow direction on ILCI results. The left-hand figure depicts the plan view of profiles relative to an ice stream flanked by two slow-flowing margins. Along the top row, schematic radargrams A-A′ to E-E′ show hypothetical internal layering recovered by radar profiles acquired at progressively lower angles to ice flow across the ice stream. The corresponding lower graph shows the magnitude of ILCI measured in a moving window spanning each profile. Importantly, the diagram shows that low ILCI, and hence disrupted internal layering, will be diagnosed at most angles, until the orientation of the profile approaches the direction of ice flow.

data acquired in spring 2009 [*Rignot et al.*, 2011]). Subsetted data sets are depicted in Figure 3a. In some parts of the IIS/MIS catchments, the filtering by ice-flow direction leaves few RES profiles to analyze, but a high concentration of RES tracks with the required directional criteria was acquired in the higher-elevation (southern) region of the survey zone (red outline in Figure 3a). We therefore focus analyses on data from this zone.

Figures 3d and 3e show ILCI results derived over 100 trace windows for RES flight tracks perpendicular to ice flow. The result is gridded at 2.5×2.5 km resolution and presented alongside the equivalent results produced from analyzing all RES flight tracks, regardless of direction, across the same region (Figures 3b and 3c). The most striking aspect of comparing Figures 3b–3e is their similarity: with the exception of a few isolated areas, the behavior of internal layers recovered from only analyzing RES profiles perpendicular to ice flow is similar to that which we would interpret from analyzing all profiles regardless of their direction.

For the equivalent analysis of ILCI calculated from the flight tracks paralleling ice flow, there are insufficient data points to grid the output meaningfully. Hence, in Figure 3f, for each location where there are coincident results both from the "perpendicular-only" and "parallel-only" experiments, i.e., at flight-track crossovers where the respective RES profiles tracked perpendicular or parallel to ice flow, we plot the sum of the parallel-only minus the perpendicular-only results. This allows us to compare the effect of flight-track direction with respect to ice flow on the ILCI calculated at each crossover. In many cases, the result of this summation is close to zero; i.e., ILCI does not change with flight-track direction. However, concentrated where ice flow is fastest, there are some instances where "parallel-to-flow" ILCI exceeds "perpendicular-to-flow" ILCI (Figure 3f), i.e., where we would interpret disrupted layering perpendicular to flow but continuous layering along flow. Our explanation for this is summarized in Figure 4 and is an extension of reasoning presented by *Ng and Conway* [2004]. Disruptions to internal layering, i.e., patterns of internal layering that diverge significantly from the ice bed and/or surface across any ice-flow route, are most often features that are inherited from ice-flow effects that have occurred further upstream. In most cases, they result from changes to the internal strain field as it passes across the margins between slower- and faster-moving ice and becomes channeled into an ice stream flow path; in some cases, the strain field is disrupted by passage of the ice over particularly large subglacial protuberances [e.g., *Hindmarsh et al.*, 2007; *Bell et al.*, 2011; *Ross et al.*, 2011]. Regardless of the specific process involved in generating the disruptions, each is directional and produces a primary axis of buckling with maximum amplitudes transverse to flow but orthogonal to which layers can appear to remain undisrupted (Figure 4 (this paper); see also *Ng and Conway* [2004]). The end result is that if one follows internal layers *directly along* an ice stream, one may observe "continuous" (undisrupted)

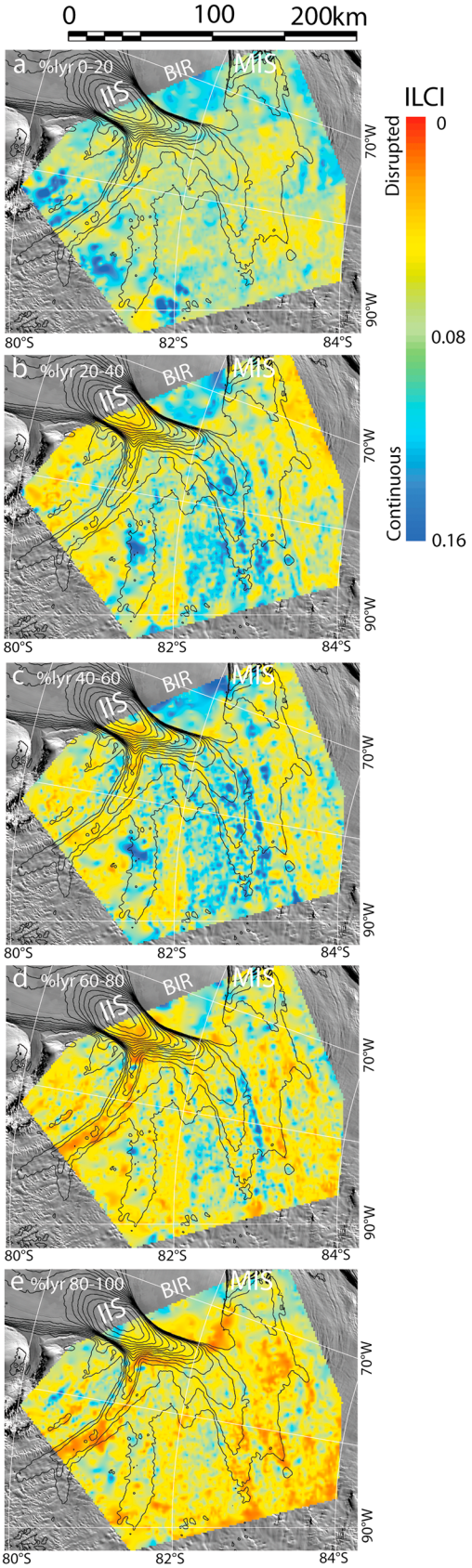

internal layering, even though RES profiles acquired in any other direction over the ice stream would show flow-disrupted internal layering. Importantly, the transition from maximum disruption across flow to minimum disruption along flow is nonlinear, such that one can still observe large disruptions to internal layering in RES profiles acquired only mildly oblique to ice flow (Figure 4). For the purposes of our study, this explains why there are occasional instances where parallel-to-flow ILCI differs from perpendicular-to-flow ILCI and why, when this occurs, it is the parallel-to-flow tracks in which we most often observe the higher ILCI (consistent with apparently continuous internal layering) and the perpendicular-to-flow ones in which we most often observe the lower ILCI (consistent with disrupted internal layering).

The critical conclusion to make is that once we discount the results from the parallel-to-flow RES tracks, the particular direction of a flight track with respect to ice flow exerts a minimal influence on the ILCI result obtained. In other words, from any given site of internal layering disruption, the ILCI value will be similar whether the flight track crosses the site perpendicular or oblique to ice flow. Only if the flight track parallels ice flow (very few cases) would the ILCI method fail to identify disruption to layers.

3.3. Variation of Internal Layering Properties With Depth

So far, we have considered the generation of single-ILCI results for each "column" of ice represented by one window of depth soundings. However, it is also possible to derive results for different depth ranges, which may be useful in searching for rapid past transitions in ice-flow regime. Evidence in support of relatively sudden changes in ice flow, as recorded by englacial features, has been reported in several cases. Notable examples are the buried crevasses underlying continuous layering in Kamb Ice Stream, evincing its stagnation ~150 years ago [*Retzlaff and Bentley*, 1993; *Catania et al.*, 2006], distinctive folding overlain by continuous layers

Figure 5. ILCI results from 100 trace moving windows partitioned by depth ranges (or "layers," abbreviated as "lyr") throughout the ice column (see text, section 3.3). (a–e) Results derived progressively downward through fifths of the ice. Background imagery and ice velocity contours as in Figure 2a. IIS = Institute Ice Stream, BIR = Bungenstock Ice Rise, and MIS = Möller Ice Stream.

interpreted as evidence for an ice-flow direction change upstream of Byrd Station in central West Antarctica [*Siegert et al.*, 2004] and buckled layering beneath continuous layers across the Bungenstock Ice Rise (BIR) [*Siegert et al.*, 2013]. To examine whether such features occur in the study region, we set up a number of experimental runs, wherein we calculated ILCI for specific ice depths.

Figure 5 shows depth-specific ILCI results for each fifth of the ice column in each 100 trace window. In Figures 5a and 5e, we plot, respectively, those lower and upper fifths of the ice column which we discarded in earlier analyses. Although some variations in internal layering in the upper fifth of the ice are discernible in Figure 5a, the overall signal is "washed out" by generally high ILCI results. These are, in fact, biased by operating the algorithm across the uppermost part of the ice column, where PASIN poorly resolves layers and produces an interference-based series of flat layers (equal to high ILCI) some way down into the ice. In Figure 5e, although a small amount of variation attributable to ice-flow processes is again discernible, this time the signal is degraded by the dominance of background noise, which has the effect of producing an apparent low ILCI. In effect, Figures 5a and 5e depict the justification for neglecting at least a proportion of the upper and lower sections of ice when applying the ILCI method, at least with PASIN-derived data.

From Figures 5b–5d, which represent ILCI in the upper two fifths, middle fifth, and lower two fifths of the ice column, respectively, the internal layering continuity across large parts of the region does not change significantly with depth. Notably, however, both in the BIR and the upstream combined IIS/MIS source tributary (~82.5°S, 80°W), there is a particularly large change from high ILCI (equal to apparently continuous layering) in the upper ice (Figures 5b and 5c) to low ILCI (equal to more disrupted layering) in the lower ice (Figure 5d). These areas therefore warrant further investigation to which we apply further analysis and discuss in the following section.

4. Discussion

4.1. Synthesis of Internal Layering and Supporting Data

From the geochronologically determined exposure times of several locations along major WSS ice stream flanks, it has been argued that ice across the western WSS has thinned steadily since the Last Glacial Maximum (LGM) [*Bentley et al.*, 2010]. Such thinning might conceivably lead to ice stream reconfigurations through impacting on subglacial hydrological routing [cf., *Retzlaff and Bentley*, 1993; *Catania et al.*, 2005; *Vaughan et al.*, 2008]. Within the downstream reaches of our study area, *Siegert et al.* [2013] interpreted a change in internal layering characteristics with depth across BIR as one line of evidence to argue that BIR may have hosted enhanced flow. This ice was probably sourced from the Ellsworth Subglacial Highlands, as part of an expanded ice sheet earlier in the Holocene. This section uses the regional internal layering database, and supporting data, to assess the extent to which this may have affected the configuration of ice flow across the much wider region encompassed by the IIS/MIS catchments.

Figure 6 presents a synthesis of depth-averaged internal layering properties, current surface ice velocities, ice thickness, and bed roughness. Across the northern reaches of the IIS catchment, encompassing the terrain dissecting the Ellsworth Subglacial Highlands, internal layering variability tends to correspond directly with the current ice-flow configuration, with low ILCI (disrupted layering) occurring where ice flow is fastest and high ILCI (apparently continuous layering) where ice flow is slow (Figure 6a). This supports the contention that ice flowing out of the Ellsworth Subglacial Highlands (generally north of 81.5°S) is highly topographically constrained and has thus maintained its spatial configuration throughout the Holocene (and possibly earlier). By contrast, much of the rest of the territory south of 81.5°S yields a weak to negligible correspondence between internal layering patterns and ice flow (Figure 6a). Assuming that most of the disruptions to the internal layering are initiated through enhanced flow processes, this might be taken as evidence of an extensive reconfiguration of ice flow relative to the present, such that regions currently experiencing slow flow contain disrupted layer signatures of paleoflow below the surface [cf., *Bingham et al.*, 2007]. However, a mitigating issue is the presence of several significant subglacial mountains in the study domain (expressed in extreme cases by nunataks, e.g., Pirrit Hills and Martin-Nash Hills), which may also act to disrupt internal layering as we now discuss.

Hindmarsh et al. [2007] demonstrated that where ice is thin relative to subglacial topography, internal layering can become warped as a consequence of ice passage over or around significant subglacial obstacles.

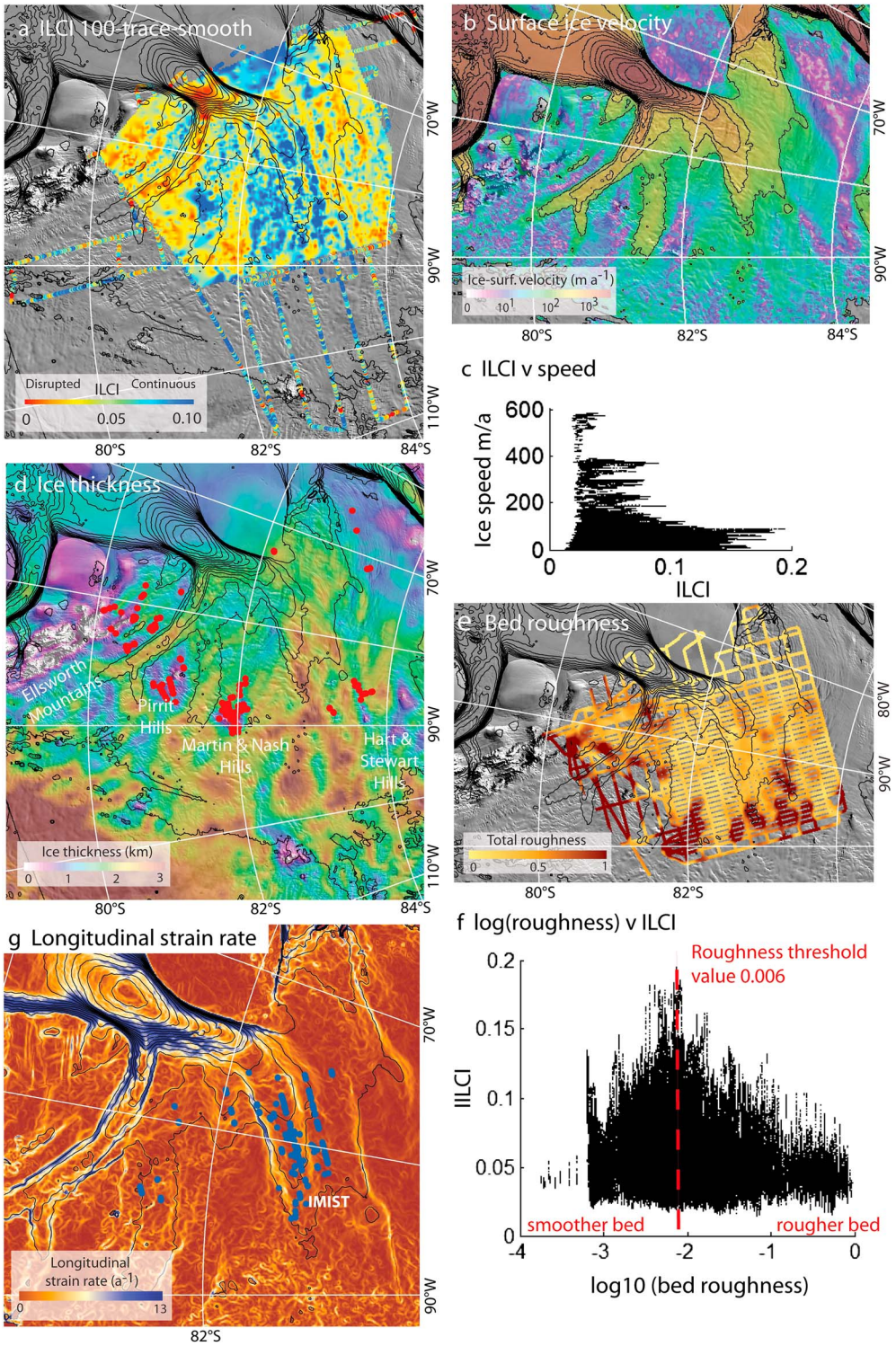

Figure 6. ILCI results compared with ice-flow velocity, ice thickness, and bed roughness. All maps include MODIS imagery [*Haran et al.*, 2006] and 25 m a^{-1} surface ice velocity contours from MEaSUREs [*Rignot et al.*, 2011]. (a) ILCI applied over 100 trace (~1 km) moving window, result gridded at 250 m resolution. (b) Surface ice velocity distribution across the catchment from measurements in 2009 [*Rignot et al.*, 2011]. (c) ILCI versus ice speed for all soundings. (d) Ice thickness map. The red points mark "unusual" locations where low ILCI (here we use ILCI < 0.03) corresponds with low ice speeds (<5 m a^{-1})—these are typically in the lee of nunataks or large subglacial mountains. (e) Distribution of total bed roughness, after *Rippin et al.* [2014]. (f) Bed roughness versus ILCI. Note the changing relationship between the two either side of the threshold roughness value $\log_{10}(-2.2) = 0.006$. (g) The color scale shows longitudinal strain rate (a^{-1}), highlighting "fingers" of greatest strain along ice stream and tributary margins. The blue points mark unusual locations where high ILCI (here we use ILCI > 0.12) corresponds with high ice speeds (>25 m a^{-1})—most are found in the central "IMIST" region.

Most of the slow-flowing regions where we retrieve "unusually" low ILCI in our study domain (red points in Figure 6d) coincide with, or are located just downstream of, significant bed perturbations such as nunataks and subglacial mountains (Figure 6d). It is also notable that at, or just downstream of, locations where bed roughness is highest (Figure 6e), the ILCI is low. Indeed, the main locations where low ILCI is measured in tandem with high bed roughness match those of low ILCI/low ice flow (Figure 6d) and are associated with internal layering being warped over or around significant subglacial protuberances. We would therefore exclude layering measured in the lee of any of the major mountain ranges, i.e., those areas characterized by cluster of red points in Figure 6c, from any interpretation of ice dynamical changes from the layer properties.

The influence on internal layering disruption of subglacial topography (as opposed to ice dynamic-induced effects) can be gauged by plotting ILCI recovered from IIS/MIS against co-located bed roughness values (Figure 6f). Here, by bed roughness, we refer to normalized total roughness values derived by Fast-Fourier-Transform analysis along sections of flight track ~320 m in length—we do not take physical meaning from the values themselves but rather pay attention to the variation between roughness values across the region [see *Rippin et al.*, 2014]. Figure 6f shows that for our study region, there is a threshold roughness value above and below, which the relationship between bed roughness and the degree of disruption to internal layering changes sign. (The roughness value at this threshold is ~0.006, but the value has no physical meaning; rather, it is the fact that there is a threshold value that is important.) Above this threshold, the mean ILCI falls (internal layering disruption increases) as bed roughness rises. For these points, we contend that ILCI is most strongly influenced by internal layering disruption as a consequence of ice flow over a rough bed. Below the threshold, mean ILCI falls with bed roughness, such that ILCI is predominantly influenced by internal flow effects—where variations in roughness are related inversely to the speed of overlying ice flow and, hence, also to the propensity for internal layering to become buckled under englacial stress gradients. Overall, the correspondence between slow ice flow/high ice flow, high bed roughness/low bed roughness, and continuous internal layering (high ILCI)/disrupted layering (low ILCI), reported from elsewhere [cf., *Bingham et al.*, 2007] generally also holds true here. However, an important conclusion from this study is that care must be taken first to discount the counter relationship caused by direct topographic disruption to internal layering. If using internal layering disruption as an indicator of ice dynamics, therefore, one should remove from consideration those regions clearly downstream of major subglacial topographic protuberances.

We also note here that we witness generally high ILCI in slow-flow areas and interstream ridges, lower ILCI in the ice streams, but the *lowest* ILCI is measured at the ice stream margins rather than in the centers of the ice streams where flow is fastest. This finding tallies with RES imaging of other ice streams [e.g., *Raymond et al.*, 2006; *King*, 2011], where while it is common to see disruption to internal layering across the entire width of ice streams, the greatest disruption to the layers is viewed across lateral shear margins, where the strain rate is greatest. It has been proposed that disruption, or buckling, of internal layering observed at any given location in an ice stream is inherited from upstream and, therefore, earlier in time [*Jacobel et al.*, 1993; *Ng and Conway*, 2004]. Convergent flow then often causes the inherited disruption to pervade toward the center of the fast-flow feature. However, where ice streams are sufficiently wide and relatively unconstrained by subglacial topography, ice flow along more or less a straight flow path can enable internal layering in the central trunk to remain relatively undisrupted over long distances. The latter scenario may explain the apparent "preservation" of unusually high ILCI in the central, >80 km wide IIS/MIS source tributary, hereafter IMIST, depicted in Figure 6g. The IMIST is currently derived from an upstream basin characterized by thick ice (Figure 6d) and a smooth bed (Figure 6e), also likely conducive to the preservation of internal layering.

4.2. Changes to Internal Layering Properties With Depth: Evidence for Ice-Flow Reconfiguration

Figure 7 displays results from depth-partitioning ILCI through tenths of the ice column. Using this partitioning, and neglecting those areas in the lee of major topographic protuberances (for the reasons discussed in section 4.1), we discriminate four styles of internal layering changes with depth across IIS/MIS as follows:

1. *Low ILCI found throughout the ice column*, diagnostic of enhanced flow disrupting internal layering. In such cases, the modern enhanced flow has disrupted layering throughout the ice column, leaving it impossible to tell whether ice flow was significantly different in the same locations previously. This category is primarily

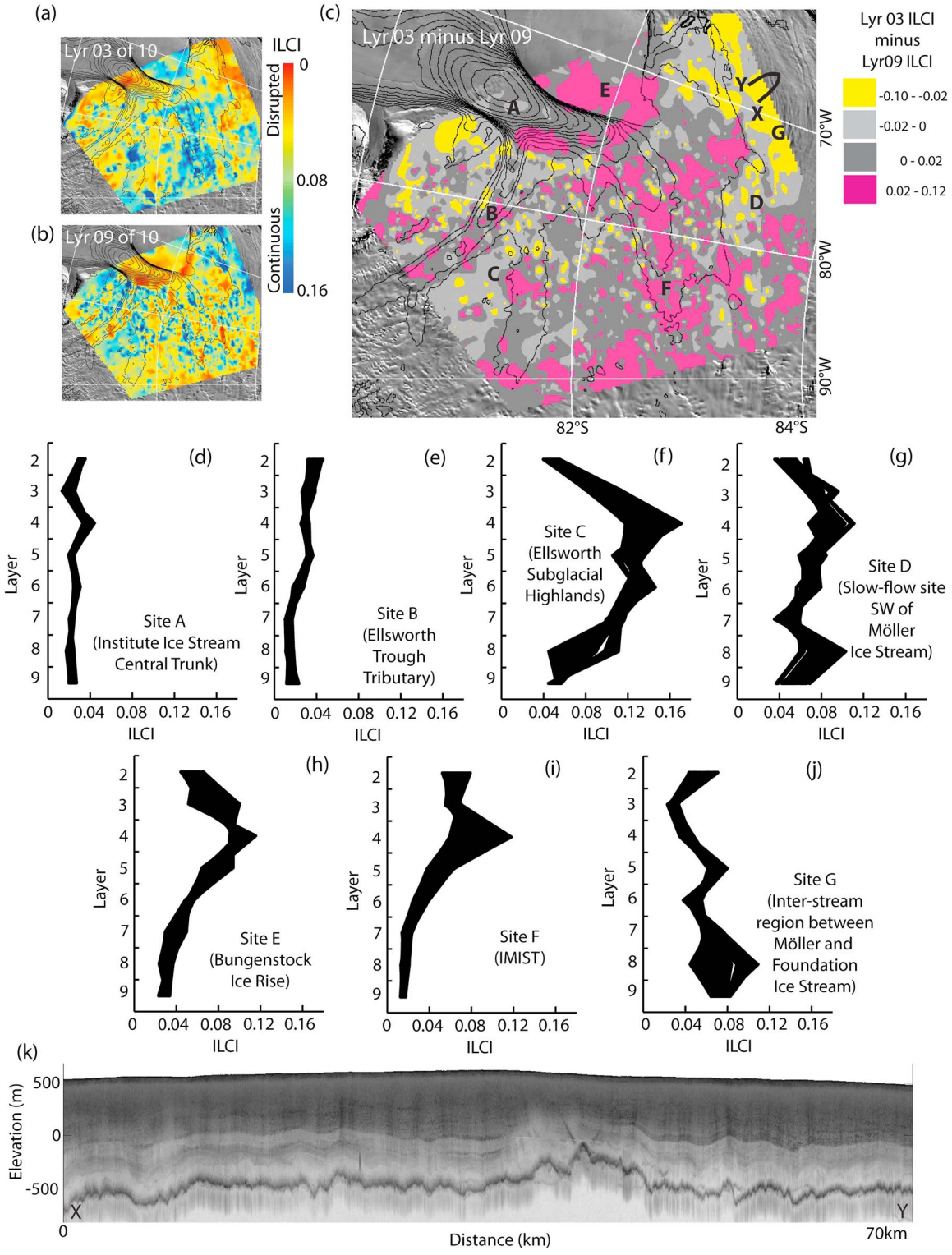

Figure 7. Results from calculating ILCI across 10 depth ranges across IIS and MIS. (a) Map of ILCI from layer 3 (relatively close to the ice surface). (b) Map of ILCI from layer 9, close to the ice bed. (c) Difference map of ILCI between layer 3 and layer 9. Cerise highlights the regions where internal layering nearer the surface is considerably less disrupted than at depth, yellow the opposite trend. (d–j) Graphs of ILCI variation with depth for 100 consecutive along-track measurements at selected locations. These span the four categories of ILCI behavior with depth discussed at the start of section 4.2, and their locations are annotated onto Figure 7c. In Figures 7d–7j, depth ranges are numbered from the ice surface downward, such that, for example, lyr 3 represents ice closer to the ice surface than lyr 9. Results for layers 1 and 10 are omitted due to noise effects discussed in section 3.3. (j) Radargram from one of the regions where deeper ice yields significantly higher ILCI than nearer-surface ice; profile location *X-Y* is given in Figure 7c.

found in the ice streams and tributaries draining the Ellsworth Subglacial Highlands and the main trunk of IIS (e.g., Figures 7d and 7e).

2. *High ILCI found throughout the ice column*, diagnostic of little disruption to either modern or paleolayering, hence indicative that no change has occurred to the ice flow. The clearest examples are found in intertributary areas of the Ellsworth Subglacial Highlands (e.g., Figures 7f and 7g).
3. *High ILCI found near the surface*, *lower ILCI deeper into the ice column*, diagnostic that enhanced flow previously occurred where there is slow flow today. A prominent example is BIR, where ILCI attains very high values in the upper three and four tenths of the ice but then falls away to lower depths (Figure 7h), supporting *Siegert et al.*'s [2013] observation of a distinct change in internal layering character at ~40% of ice depth. In the upper parts of the IIS and MIS catchments, and especially in the IMIST, we also observe slightly higher ILCI in upper layers than in the deeper layers (e.g., Figure 7i); however, the range of ILCI values is much smaller than observed across BIR, and nowhere is the decline in ILCI with depth as large as it is across BIR.
4. *Low ILCI found near the surface*, *higher ILCI deeper into the ice column*. These cases are primarily found in lower MIS, the upland regions between MIS and Foundation Ice Stream, and over subglacial mountains northwest of IIS's main trunk and are discussed further below (e.g., Figure 7j).

Of the above, case 3 is the most informative in terms of providing empirical evidence for changes in ice-flow configuration across IIS/MIS. The englacial patterns recovered across the study region are consistent with the Late Holocene shutdown of ice flow over BIR hypothesized by *Siegert et al.* [2013] and hint at the wider impacts the attendant reconfiguration of ice flow has had across much of IIS and MIS. Only the northern sector of IIS, being topographically constrained as it flows through the Ellsworth Subglacial Highlands, shows no evidence of a major reconfiguration of flow paths, with disrupted internal layering at all depths in its ice stream tributaries. It is very likely that higher-than-present ice flux passed through these tributaries, notably the Ellsworth Trough Tributary, earlier in the Holocene [*Bentley et al.*, 2010; *Ross et al.*, 2011; *Siegert et al.*, 2013] and drove the enhanced flow across BIR. Ice from this sector is today directed northeastward to the FRIS via IIS's main trunk before reaching BIR. It is therefore probable that activation of IIS's main trunk occurred as BIR stagnated, in turn inducing switches in ice flow routing throughout the upper regions of IIS and MIS, especially in the IMIST region. The observed transition in some parts of IMIST from more disrupted layering at depth to more continuous layers nearer the surface (e.g., Figure 7i) could have occurred as ice stream tributary boundaries migrated to accommodate this new connection to the FRIS. Future work underpinned by catchment-wide tracing of internal layers, and potentially the linking of some of these layers with dated horizons linked to ice cores, is required to constrain the timing of these changes.

The instances of higher ILCI ice underlying lower ILCI ice, exemplified by ice in lower MIS, the upland regions between MIS and Foundation Ice Stream, and over subglacial mountains northwest of IIS's main trunk (Figures 7c and 7j), are less explicable through ice dynamic considerations. In most of the radar profiles where this trend is identified, the lower ice displays a notably different character to the upper ice, being characterized by a distinct transition in the brightness of internal layers at ~60% of ice depth (e.g., Figure 7k). The cause of this phenomenon is a topic for further investigation but, we suggest, is likely linked to ice fabric. One possibility is that the lower ice package manifests ice with preferred crystal orientations developed during passage over significant subglacial obstacles [*Siegert and Kwok*, 2000; *Ross and Siegert*, 2014]. Another is that the transition reflects contrasting physical properties associated with the palaeoclimatic switch from glacial to interglacial accumulation-driven ice-crystal formation [cf., *Paterson*, 1991; *Durand et al.*, 2007; *Kennedy et al.*, 2013; *Montagnat et al.*, 2014].

5. Conclusions

We have analyzed in detail the patterns of radio echo-sounded internal ice sheet layering within the Institute and Möller Ice Streams (IIS and MIS), West Antarctica. We identified spatial organization in the properties of internal layering across IIS and MIS, yet the overall correspondence with current ice-surface velocities as recovered from satellite data, and ice-bed roughness, is not straightforward. A correspondence between internal layering continuity/disruption, slow flow/fast flow, and high/low bed roughness is found in the ice draining through well-defined troughs from the Ellsworth Subglacial Highlands to IIS. Analysis of internal

layering properties with respect to different ice depths suggests that this situation has prevailed there throughout at least the Holocene. Further south and east, in the upper reaches of IIS and MIS, variation of internal layering with depth occurs in a manner inconsistent with modern (surface) ice flow. The internal layering continuity often changes with depth across these upstream regions, frequently with more disrupted layering being overlain by more continuous layering nearer the surface. Our results provide support for the assertion that major ice-flow pathways feeding IIS and MIS have been subjected to substantial dynamic and/or directional changes during the Holocene, enabled by a lack of significant controlling topography south of the Ellsworth Subglacial Highlands. The Late Holocene deceleration of flow across the Bungenstock Ice Rise previously inferred by *Siegert et al.* [2013] may therefore represent just one relatively local component of wider regional changes to ice flow that have occurred across the IIS/MIS catchments as the WAIS has thinned since the LGM.

A useful next stage to the work presented here would be to investigate possibilities for implementing dating control to the internal layering across IIS and MIS, using radar layers tied to the nearest ice core age-depth profiles [e.g., *West Antarctic Ice Sheet Divide Project Members*, 2013], thereby to investigate the catchment-wide timing of the dynamic reconfiguration(s). Such efforts will support the wider goal of reconstructing the Holocene glacial history of the Weddell Sea sector [e.g., *Hillenbrand et al.*, 2014].

Acknowledgments

Data used for this article are available at the NERC Airborne Geophysics Data Portal https://secure.antarctica.ac.uk/data/aerogeo/. Funding was provided by NERC Antarctic Funding Initiative (reference NE/G013071/1). We thank the operational and logistical staff of British Antarctic Survey for field support, Carl Robinson (airborne survey engineer), Doug Cochrane and Ian Potten (pilots), and Mark Oostlander (air mechanic) for their invaluable survey support. Finally, we thank the Scientific Editor E. C. Pettit, R. W. Jacobel, R. Drews and an anonymous reviewer for constructive comments which improved the manuscript.

References

Anandakrishnan, S., D. D. Blankenship, R. B. Alley, and P. L. Stoffa (1998), Influence of subglacial geology on the position of a West Antarctic ice stream from seismic observations, *Nature*, *394*, 62–65, doi:10.1038/27889.

Bell, R. E., et al. (2011), Widespread persistent thickening of the East Antarctic Ice Sheet by freezing from the base, *Science*, *331*, 1592–1595, doi:10.1126/science.1200109.

Bentley, M. J., C. J. Fogwill, A. M. Le Brocq, A. L. Hubbard, D. E. Sugden, T. J. Dunai, and S. P. H. T. Freeman (2010), Deglacial history of the West Antarctic Ice Sheet in the Weddell Sea embayment: Constraints on past ice volume change, *Geology*, *38*, 411–414, doi:10.1130/G30754.1.

Bindschadler, R. A., et al. (2011), Getting around Antarctica: New high-resolution mappings of the grounded and freely floating boundaries of the Antarctic ice sheet created for the International Polar Year, *Cryosphere*, *5*, 569–588, doi:10.5194/tc-5-569-2011.

Bingham, R. G., and M. J. Siegert (2007), Bed roughness characterization of Institute and Möller Ice Streams, West Antarctica: Comparison with Siple Coast ice streams, *Geophys. Res. Lett.*, *34*, L21504, doi:10.1029/2007GL031483.

Bingham, R. G., and M. J. Siegert (2009), Quantifying subglacial bed roughness in Antarctica: Implications for ice-sheet dynamics and history, *Quat. Sci. Rev.*, *28*, 223–239, doi:10.1016/j.quascirev.2008.10.014.

Bingham, R. G., M. J. Siegert, D. A. Young, and D. D. Blankenship (2007), Organized flow from the South Pole to the Filchner-Ronne Ice Shelf: An assessment of balance velocities in interior East Antarctica using radio echo sounding data, *J. Geophys. Res.*, *112*, F03S26, doi:10.1029/2006JF000556.

Brunt, K., H. A. Fricker, and L. Padman (2011), Analysis of ice plains of Filchner/Ronne Ice Shelf, Antarctica, using ICESat laser altimetry, *J. Glaciol.*, *57*, 965–975, doi:10.3189/002214311798043753.

Catania, G. A., H. Conway, C. F. Raymond, and T. A. Scambos (2005), Surface morphology and internal layer stratigraphy in the downstream end of Kamb Ice Stream, West Antarctica, *J. Glaciol.*, *51*, 423–431, doi:10.3189/172756505781829142.

Catania, G. A., T. A. Scambos, H. Conway, and C. F. Raymond (2006), Sequential stagnation of Kamb Ice Stream, West Antarctica, *Geophys. Res. Lett.*, *33*, L14502, doi:10.1002/9781118782033.ch24.

Conway, H., G. Catania, C. F. Raymond, A. M. Gades, T. A. Scambos, and H. Engelhardt (2002), Switch of flow direction in an Antarctic ice stream, *Nature*, *419*, 465–467, doi:10.1038/nature01081.

Corr, H. F. J., F. Ferraccioli, N. Frearson, T. Jordan, C. Robinson, E. Armadillo, G. Caneva, E. Bozzo, and I. Tabacco (2007), Airborne radio echo sounding of the Wilkes Subglacial Basin, the Transantarctic Mountains, and the Dome C region, *Terra Antart. Rep.*, *13*, 55–63.

Durand, G., F. Gillet-Chaulet, A. Svensson, O. Gagliardini, S. Kipfstuhl, J. Meysonnier, F. Parrenin, P. Duval, and D. Dahl-Jensen (2007), Change in ice rheology during climate variations: Implications for ice flow modeling and dating of the EPICA Dome C core, *Clim. Past*, *3*, 155–167, doi:10.5194/cp-3-155-2007.

Echelmeyer, K., and W. H. Harrison (1999), Ongoing margin migration of Ice Stream B, Antarctica, *J. Glaciol.*, *45*, 361–369, doi:10.3189/002214399793377059.

Eisen, O., I. Hamann, S. Kipfstuhl, D. Steinhage, and F. Wilhelms (2007), Direct evidence for continuous radar reflector originating from changes in crystal-orientation fabric, *Cryosphere*, *1*, 1–10, doi:10.5194/tc-1-1-2007.

Favier, L., G. Durand, S. L. Cornford, G. H. Gudmundsson, O. Gagliardini, F. Gillet-Chaulet, T. Zwinger, A. J. Payne, and A. M. Le Brocq (2014), Retreat of Pine Island Glacier controlled by marine ice-sheet instability, *Nature Clim. Change*, *4*, 117–121, doi:10.1038/nclimate2094.

Flament, T., and F. Rémy (2012), Dynamic thinning of Antarctic glaciers from along-track repeat radar altimetry, *J. Glaciol.*, *58*, 830–840, doi:10.3189/2012JoG11J118.

Fretwell, P. T., et al. (2013), Bedmap2: Improved ice bed, surface, and thickness datasets for Antarctica, *Cryosphere*, *7*, 375–393, doi:10.5194/tc-7-375-2013.

Gudlaugsson, E., A. Humbert, M. Winsborrow, and K. Andreassen (2013), Subglacial roughness of the former Barents Sea Ice Sheet, *J. Geophys. Res. Earth Surf.*, *118*, 2546–2556, doi:10.1002/2013JF002714.

Haran, T., J. Bohlander, T. Scambos, T. Painter, and M. Fahnestock (2006), *MODIS Mosaic Image of Antarctica*, National Snow and Ice Data Center, Digital media, Boulder, Colo.

Hélière, F., C.-C. Lin, H. Corr, and D. Vaughan (2007), Radio echo sounding of Pine Island Glacier, West Antarctica: Aperture synthesis processing and analysis of feasibility from space, *IEEE Trans. Geosci. Remote Sens.*, *45*, 2573–2582, doi:10.1109/TGRS.2007.897433.

Hellmer, H. H., F. Kauker, R. Timmermann, J. Determann, and J. Rae (2012), Twenty-first-century warming of a large Antarctic ice-shelf cavity by a redirected coastal current, *Nature*, *485*, 225–228, doi:10.1038/nature11064.

Hempel, L., F. Thyssen, N. Gundestrup, H. B. Clausen, and H. Miller (2000), A comparison of radio echo sounding data and electrical conductivity of the GRIP ice core, *J. Glaciol.*, *46*, 369–374, doi:10.3189/172756500781833070.
Hillenbrand, C.-D., et al. (2014), Reconstruction of changes in the Weddell Sea sector of the Antarctic Ice Sheet since the Last Glacial Maximum, *Quat. Sci. Rev.*, *100*, 111–136, doi:10.1016/j.quascirev.2013.07.020.
Hindmarsh, R. C. A., G. J.-M. C. Leysinger Vieli, M. J. Raymond, and G. H. Gudmundsson (2007), Draping or overriding: The effect of horizontal stress gradients on internal layer architecture in ice sheets, *J. Geophys. Res.*, *111*, F02018, doi:10.1029/2005JF000309.
Jacobel, R. W., A. M. Gades, D. L. Gottschling, S. M. Hodge, and D. L. Wright (1993), Interpretation of radar-detected internal layer folding in West Antarctic ice streams, *J. Glaciol.*, *39*, 528–537.
Jacobel, R. W., T. A. Scambos, C. F. Raymond, and A. M. Gades (1996), Changes in the configuration of ice stream flow from the West Antarctic Ice Sheet, *J. Geophys. Res.*, *101*, 5499–5504, doi:10.1029/95JB03735.
Jordan, T. A., F. Ferraccioli, N. Ross, H. F. J. Corr, P. T. Leat, R. G. Bingham, D. M. Rippin, A. M. Le Brocq, and M. J. Siegert (2013), Inland extent of the Weddell Sea Rift imaged by new aerogeophysical data, *Tectonophysics*, *585*, 137–160, doi:10.1016/j.tecto.2012.09.010.
Joughin, I., and R. B. Alley (2011), Stability of the West Antarctic Ice Sheet in a warming world, *Nat. Geosci.*, *4*, 506–513, doi:10.1038/ngeo1194.
Karlsson, N. B., D. M. Rippin, R. G. Bingham, and D. G. Vaughan (2012), A "continuity-index" for assessing ice-sheet dynamics from radar-sounded internal layers, *Earth Planet. Sci. Lett.*, *335-336*, 88–94, doi:10.1016/j.epsl.2012.04.034.
Karlsson, N. B., R. G. Bingham, D. M. Rippin, R. C. A. Hindmarsh, H. F. J. Corr, and D. G. Vaughan (2014), Constraining past accumulation in the central Pine Island Glacier basin using radio echo sounding, *J. Glaciol.*, *60*, 553–562, doi:10.3189/2014JoG13J180.
Kennedy, J. H., E. C. Pettit, and C. L. Di Prinzio (2013), The evolution of crystal fabric in ice sheets and its link to climate history, *J. Glaciol.*, *59*, 357–373, doi:10.3189/2013JoG12J159.
King, E. C. (2011), Ice stream or not? Radio echo sounding of Carlson Inlet, West Antarctica, *Cryosphere*, *5*, 907–916, doi:10.5194/tc-5-907-2011.
Leysinger Vieli, G. J.-M. C., R. C. A. Hindmarsh, M. J. Siegert, and S. Bo (2011), Time-dependence of the spatial pattern of accumulation rate in East Antarctica deduced from isochronic radar layers using a 3-D numerical ice flow model, *J. Geophys. Res.*, *116*, F02018, doi:10.1029/2010JF001785.
MacGregor, J. A., K. Matsuoka, M. R. Koutnik, E. D. Waddington, M. Studinger, and D. P. Winebrenner (2009), Millennially averaged accumulation rates for the Vostok Subglacial Lake region inferred from deep internal layers, *Ann. Glaciol.*, *50*, 25–34, doi:10.3189/172756409789097441.
McMillan, M., A. Shepherd, A. Sundal, K. Briggs, A. Muir, A. Ridout, A. Hogg, and D. J. Wingham (2014), Increased ice losses from Antarctica detected by CryoSat-2, *Geophys. Res. Lett.*, *41*, 3899–3905, doi:10.1002/2014GL060111.
Moholdt, G., H. A. Fricker, and L. Padman (2012), Lagrangian analysis of ICESat altimetry reveals patterns of ice shelf basal melting, Abstract C41E-06 presented at 2012 Fall Meeting, AGU, San Francisco, Calif., 3–7 Dec.
Montagnat, M., N. Azuma, D. Dahl-Jensen, J. Eichler, S. Fujita, F. Gillet-Chaulet, S. Kipfstuhl, D. Samyn, A. Svensson, and I. Weikusat (2014), Fabric along the NEEM ice core,Greenland, and its comparison with GRIP and NGRIP ice cores, *Cryosphere*, *8*, 1129–1138, doi:10.5194/tc-8-1129-2014.
Moore, J. (1988), Dielectric variability of a 130 m Antarctic ice core: Implications for radar sounding, *Ann. Glaciol.*, *11*, 95–99.
Neumann, T. A., H. Conway, S. F. Price, E. D. Waddington, G. A. Catania, and D. L. Morse (2008), Holocene accumulation and ice sheet dynamics in central West Antarctica, *J. Geophys. Res.*, *113*, F02018, doi:10.1029/2007JF000764.
Ng, F., and H. Conway (2004), Fast-flow signature in the stagnated Kamb Ice Stream, West Antarctica, *Geology*, *32*, 481–484, doi:10.1130/G20317.1.
Paterson, W. S. B. (1991), Why ice-age ice is sometimes "soft", *Cold Reg. Sci. Technol.*, *20*, 75–98, doi:10.1016/0165-232X(91)90058-O.
Peters, L. E., S. Anandakrishnan, R. B. Alley, J. P. Winberry, D. E. Voigt, A. M. Smith, and D. L. Morse (2006), Subglacial sediments as a control on the onset and location of two Siple Coast ice streams, West Antarctica, *J. Geophys. Res.*, *111*, B01302, doi:10.1029/2005JB003766.
Pritchard, H. D., R. J. Arthern, D. G. Vaughan, and L. A. Edwards (2009), Extensive dynamic thinning on the margins of the Antarctic and Greenland Ice Sheets, *Nature*, *461*, 971–975, doi:10.1038/nature08471.
Pritchard, H. D., S. R. M. Ligtenberg, H. A. Fricker, D. G. Vaughan, M. R. van den Broeke, and L. Padman (2012), Antarctic ice-sheet loss driven by basal melting of ice shelves, *Nature*, *484*, 502–505, doi:10.1038/nature10968.
Raymond, C. F., G. A. Catania, N. Nereson, and C. J. van der Veen (2006), Bed radar reflectivity across the north margin of Whillans Ice Stream, West Antarctica, and implications for margin processes, *J. Glaciol.*, *52*, 3–10, doi:10.3189/172756506781828890.
Retzlaff, R., and C. R. Bentley (1993), Timing of stagnation of Ice Stream C, West Antarctica, from short-pulse radar studies of buried surface crevasses, *J. Glaciol.*, *39*, 553–561.
Rignot, E., J. Mouginot, and B. Scheuchl (2011), Ice flow of the Antarctic ice sheet, *Science*, *333*, 1427–1430, doi:10.1126/science.1208336.
Rippin, D. M., M. J. Siegert, and J. L. Bamber (2003), The englacial stratigraphy of Wilkes Land, East Antarctica, as revealed by internal radio echo sounding layering, and its relationship with balance velocities, *Ann. Glaciol.*, *36*, 189–196, doi:10.3189/172756403781816356.
Rippin, D. M., R. G. Bingham, T. A. Jordan, A. P. Wright, N. Ross, H. F. J. Corr, F. Ferraccioli, A. M. Le Brocq, K. C. Rose, and M. J. Siegert (2014), Basal roughness of the Institute and Möller Ice Streams, West Antarctica: Determining past ice-dynamical regimes, *Geomorphology*, *214*, 139–147, doi:10.1016/j.geomorph.2014.01.021.
Ross, N., and M. Siegert (2014), Concentrated englacial shear over rigid basal ice, West Antarctica: Implications for modeling and ice sheet flow, *Geophys. Res. Abstr.*, *16*, EGU2014–5568.
Ross, N., M. J. Siegert, J. Woodward, A. M. Smith, H. F. J. Corr, M. J. Bentley, R. C. A. Hindmarsh, E. C. King, and A. Rivera (2011), Holocene stability of the Amundsen-Weddell ice divide, West Antarctica, *Geology*, *39*, 935–938, doi:10.1130/G31920.1.
Ross, N., R. G. Bingham, H. F. J. Corr, F. Ferraccioli, T. A. Jordan, A. M. Le Brocq, D. M. Rippin, D. A. Young, D. D. Blankenship, and M. J. Siegert (2012), Steep reverse bed slope at the grounding line of the Weddell Sea sector in West Antarctica, *Nat. Geosci.*, *5*, 393–396, doi:10.1038/ngeo1468.
Scambos, T., J. Bohlander, B. Raup, and T. Haran (2004), Glaciological characteristics of Institute Ice Stream using remote sensing, *Antarctic Sci.*, *16*, 205–213, doi:10.1017/S0954102004001.
Schoof, C. (2007), Ice sheet grounding line dynamics: Steady states, stability, and hysteresis, *J. Geophys. Res.*, *112*, F03S28, doi:10.1029/2006JF000664.
Siegert, M. J., and S. Fujita (2001), Internal ice-sheet radar layer profiles and their relation to reflection mechanisms between Dome C and the Transantarctic Mountains, *J. Glaciol.*, *47*, 205–212, doi:10.3189/172756501781832205.
Siegert, M. J., and R. Kwok (2000), Ice-sheet radar layering and the development of preferred crystal orientation fabrics between Lake Vostok and Ridge B, central East Antarctica, *Earth Planet. Sci. Lett.*, *179*, 227–235, doi:10.1016/S0012-821X(00)00121-7.
Siegert, M. J., and A. J. Payne (2004), Past rates of accumulation in central West Antarctica, *Geophys. Res. Lett.*, *31*, L12403, doi:10.1029/2004GL020290.
Siegert, M. J., A. J. Payne, and I. Joughin (2003), Spatial stability of Ice Stream D and its tributaries, West Antarctica, revealed by radio echo sounding and interferometry, *Ann. Glaciol.*, *37*, 377–382, doi:10.3189/172756403781816022.

Siegert, M. J., B. Welch, D. Morse, A. Vieli, D. D. Blankenship, I. Joughin, E. C. King, G. J.-M. C. Leysinger Vieli, A. J. Payne, and R. Jacobel (2004), Ice flow direction change in interior West Antarctica, *Science*, *24*, 1948–1951, doi:10.1038/nature01081.

Siegert, M., N. Ross, H. Corr, J. Kingslake, and R. Hindmarsh (2013), Late Holocene ice-flow reconfiguration in the Weddell Sea sector of West Antarctica, *Quat. Sci. Rev.*, *78*, 98–107, doi:10.1016/j.quascirev.2013.08.003.

Tulaczyk, S., W. B. Kamb, and H. F. Engelhardt (2000), Basal mechanics of ice stream B, West Antarctica: 1. Till mechanics, *J. Geophys. Res.*, *105*, 463–481, doi:10.1029/1999JB900329.

Vaughan, D. G., H. F. J. Corr, A. M. Smith, H. D. Pritchard, and A. Shepherd (2008), Flow-switching and water piracy between Rutford Ice Stream and Carlson Inlet, West Antarctica, *J. Glaciol.*, *54*, 41–48, doi:10.3189/002214308784409125.

Vaughan, D. G., et al. (2013), Observations: Cryosphere, in *Climate Change 2013: The Physical Science Basis*, Cambridge Univ. Press, Cambridge, U. K., and New York.

Waddington, E. D., T. A. Neumann, M. R. Koutnik, H.-P. Marshall, and D. L. Morse (2007), Inference of accumulation-rate patterns from deep radar layers in glaciers and ice sheets, *J. Glaciol.*, *53*, 694–712, doi:10.3189/002214307784409351.

West Antarctic Ice Sheet Divide Project Members (2013), Onset of deglacial warming in West Antarctica driven by local orbital forcing, *Nature*, *500*, 440–444, doi:10.1038/nature12376.

Woodward, J., and E. C. King (2009), Radar surveys of the Rutford Ice Stream onset zone, West Antarctica: Indications of flow (in)stability, *Ann. Glaciol.*, *50*(51), 57–62, doi:10.3189/172756409789097469.

Journal of Geophysical Research – Earth Surface

Supporting Information for

Ice-flow structure and ice-dynamic changes in the Weddell Sea sector of West Antarctica from radar-imaged internal layering

Robert G. Bingham[1*], David M. Rippin[2], Nanna B. Karlsson[3], Hugh F.J. Corr[4], Fausto Ferraccioli[4], Tom A. Jordan[4], Anne M. Le Brocq[5], Kathryn C. Rose[6], Neil Ross[7] and Martin J. Siegert[8]

*corresponding author, email: r.bingham@ed.ac.uk

1.School of GeoSciences, University of Edinburgh, UK.

2. Environment Department, University of York, UK.

3. Centre for Ice and Climate, Niels Bohr Institute, University of Copenhagen, Denmark.

4.British Antarctic Survey, Natural Environment Research Council, Cambridge, UK.

5.Geography, College of Life and Environmental Sciences, University of Exeter, UK.

6.Bristol Glaciology Centre, School of Geographical Sciences, University of Bristol, UK.

7. School of Geography, Politics and Sociology, Newcastle University, UK.

8. Grantham Institute and Department of Earth Science and Engineering, Imperial College London, UK.

Contents of this file

Introduction

This supplement takes the form of three sections of text introducing (S1.1) the Internal Layering Continuity Index (ILCI) methodology that is used in the accompanying paper, (S1.2) a presentation of the main considerations the user must take into account before application, and (S1.3) a discussion of the effects of moving-window size on the results. Figure S1 is presented in support of the text in Section S1.3.

S1.1 Internal Layering Continuity Index

The Internal-Layering Continuity Index (ILCI) deployed here was first presented by *Karlsson et al.* [2012] and applied to Pine Island Glacier, and it has also been applied to RES data from Greenland [*Sime et al.*, 2014]. ILCI builds upon previous manual classifications of internal layering "types" from older, non-digital, RES data, in which layering was classified as either "continuous" or "disrupted/buckled" depending on the degree to which it accorded with the ice surface and bed [e.g. *Siegert et al.*, 2003; *Rippin et al.*, 2003; *Bingham et al.*, 2007]. This, in turn, was held to reflect the degree to which layering has been modified, by ice dynamics, from the initial "continuous" internal layers laid down by paleo-accumulation events. While this manual classification system was necessary for older analogue RES datasets, large digital datasets such as those acquired for this study can be more readily analyzed using automated processing such as the ILCI technique. It is important to note, however, that though results can be generated rapidly, their interpretation still requires validation and knowledge of the limitations of the technique, as we shall describe below. Throughout this appendix and the preceding paper, we follow *Karlsson et al.* [2012] in that "continuity" in the term ILCI refers to the degree to which internal layering is apparently "continuous" in being traceable over large distances as in the classification system describe above.

The ILCI is derived by examining individual traces (often termed "A-scope format; see Fig. 2e&f of this paper, and *Karlsson et al.* [2012]'s Fig. 1) along each RES flight track. More specifically with this dataset, each "trace" represents a stack of ten consecutive raw traces, imposed during 2-D SAR-focussing to minimize noise, but no further processing steps were undertaken prior to applying the ILCI. Considering an individual trace from anywhere along a RES profile, high and low amplitudes in relative reflected power with time through the ice column reflect passage of that trace across boundaries of dielectric contrast. In an area of ice in which internal layering is "continuous" or "well-preserved" (using the terminology above), individual traces are characterized by high-amplitude fluctuations (e.g. this paper, Fig. 2f). By contrast, where internal layers are more "disrupted," or absent, dielectric contrasts in the individual traces are less marked, bringing about lower-amplitude fluctuations in relative reflected power with depth (e.g. this paper, Fig. 2e). These variations can be quantified by calculating the trace-specific ILCI, ψ, as

$$\psi = \frac{1}{2\Delta r N} \sum_{i=n_1}^{n_N} [P_{i+1} - P_{i-1}]$$

where P_i is the reflected relative power (dB) at point *i*, $N \equiv n_1 : n_N$ is used to describe the total number of relative reflected power values being analyzed between a predefined upper and lower limits within the ice column, and Δr is the depth interval which can be any vertical coordinate (two-way travel time, distance, or image pixels). The extreme upper and lower limits are the ice surface and the ice-bed interface respectively, though sensitivity experiments discussed in *Karlsson et al.* [2012] have demonstrated that discarding a proportion of the upper and lower ice column from the analysis is prudent. This upper part is discarded because it is dominated by density differences not resolved well by the PASIN 150 MHz system. The lower part is discarded because it often contains little to no layering, perhaps because layers have been too disrupted by high strain rates already, and/or may be affected significantly by variable attenuation across the catchment scale (as further discussed in Section S1.2) .

Because our primary interest with this paper lies in interpreting regional-scale change in the WSS catchments, our interest is not in trace-specific values of ψ per se; rather it is in how ψ changes across the region. Consequently, to apply ILCI regionally,

we average ψ over moving windows along flight tracks. An example is given by *Karlsson et al.*'s [2012] application of ILCI to Pine Island Glacier. There, where ice flow is slow internal layers are imaged as continuous features and the ILCI is high; where ice flow is fast and internal layers are highly disrupted or even absent, the ILCI is lower. Across the Pine Island Glacier catchment, the ILCI distribution closely corresponds with the present-day ice-flow configuration, supporting the contention that this configuration has remained stable over the history of the ice, presumably due to topographic constraints [*Vaughan et al.*, 2006]. Critically, however, where topography is less controlling, past ice-flow migrations, known to have taken place elsewhere in Antarctica, may leave signals of internal-layering disruption in the ice that do not match the current ice-flow configuration [c.f. *Bingham et al.*, 2007; *Woodward and King*, 2009; *Siegert et al.*, 2013]. ILCI mapped across ice catchments and analyzed with supplementary evidence, such as contemporary maps of ice flow, therefore offers potential for identification of any historical changes to ice-flow.

S1.2 Important factors to consider when deploying ILCI

It is important to be clear that what is measured directly by ILCI is, firstly, variations in dielectric contrast through individual traces, which are then, secondly, averaged over adjacent traces, the number of which is given by the size of the moving analysis window. Strictly speaking then, ILCI does not *directly* measure continuity of signal between adjacent traces, but in practice (and having been applied across several parts of Antarctica and Greenland [e.g., *Karlsson et al.*, 2012; *Sime et al.*, 2014; and this paper] acts as an effective proxy for continuity of signal between adjacent traces. This distinction is important, especially for low values of ILCI, because there are other factors which may reduce dielectric contrasts other than disruption to internal layering. One example is spatial aliasing of RES returns in areas of steep layer slopes, where a proportion of the return is missed by the receiver resulting in apparent weakening of dielectric contrast per trace. Aliasing of layer returns may therefore act to reduce the retrieved ILCI, where there may, in fact, be good continuity of layering from trace to trace. Validating results with visual inspection and taking into account layer slopes in any interpretation can ameliorate this issue. However, the issue becomes proportionately less influential with increasing ILCI analysis-window size. Another example is that attenuation of RES signal with depth may vary significantly in ice of varying speed, fabric and/or temperature [*Matsuoka*, 2011], and we must be therefore be cautious in overinterpreting any variations in signal fading at depth. This is one reason we neglect ILCI signals from the very lowest ice depths. Aliasing of RES signals is affected both by the acquisition frequency and sampling density, while signal attenuation is also frequency dependent. For this reason we do not recommend ILCI results be directly compared between studies unless the data were acquired and processed with exactly the same parameters. Similarly, depending on the purpose of an individual study, different moving-window sizes may be appropriate, and an important first step in using ILCI is to undertake experiments to determine which is most appropriate for a given site/study aim. Hence we do not, in this study, make any direct comparisons between the ILCI values we have acquired across IIS/MIS relative to those from Pine Island Glacier (as reported by *Karlsson et al.* [2012]).

S1.3. Optimizing moving-window size

A preliminary analytical step for this study was to identify an ILCI moving-window size appropriate for mapping internal layering patterns across IIS and MIS. In the work on Pine Island Glacier, for example, *Karlsson et al.* [2012] experimented with various moving-window sizes and plot the results of using 100 traces (~3 km, or ~1-2 ice thicknesses) versus 1000 traces (~30 km, or ~10 ice thicknesses) [*Karlsson et al.*, 2012, their Fig. 3]. In that work and here, preliminary tests demonstrated that if the window is made too small results will contain too much noise; if it is too large then the variations we wish to identify become averaged out to the point of extinction. Fig. S1 shows the ILCI derived for varying moving-window sizes. We derived results for moving-window sizes of 20, 50, 100, 200 and 1000 consecutive traces along flight tracks, respectively approximating to 0.2, 0.5, 1, 2 and 10 km, or 0.01-0.05, 0.25-0.5, 0.5-1, 1-2 and 5-10 ice thicknesses. All results shown in Fig. 3 were produced from application of the ILCI to the middle 3/5 of the ice column; as found in *Karlsson et al.* [2012], and also in further preliminary sensitivity experiments with these data, we determined that omitting the upper and lower fifths of the ice column, which often contain few or no resolved layers, removes noise.

In Fig. S1a we plot the ILCI results from 100-trace windowing along the flight tracks, with the result for each window plotted at its centerpoint. In the lower-elevation (northeast) sector of IIS, and also within the dissected terrain draining from the Ellsworth Subglacial Highlands, we readily observe a strong correspondence between high depth-averaged ILCI and slow ice flow, and low depth-averaged ILCI with tributary and ice-stream (faster) flow. Moreover, ILCI results derived from parallel flight tracks tend to display matching trends of ILCI variation and, zooming in to any given flight track, it is additionally notable that variations in ILCI often correspond with changes in surface properties visible in satellite imagery (Fig. A1b).

Fig. S1a presents much information, but as an interpretative tool is best viewed and interrogated interactively, rather than as in the single 'screen-shot' depicted. As a way of more effectively summarizing the findings, we gridded results across the survey region (Fig S1c-f); a process facilitated by the regular spacing and orientation of the flight tracks. Grid-cell size is an important variable here: we must not overinterpolate between flight tracks, nor degrade too much the detailed information along flight tracks. Sensitivity tests showed that gridding results to 2.5 km^2 grid cells produces a reasonable offset between these limitations.

Our main finding in terms of determining the best ILCI moving-window size to use for this study is that windows of ~100 traces (≈ 1-2 ice thicknesses) offer the best offset between introducing too much noise into the ILCI signal (window sizes that are too small) or losing signal with too much averaging (window sizes that are larger). In our further experiments we therefore proceeded with using 100-trace moving windows.

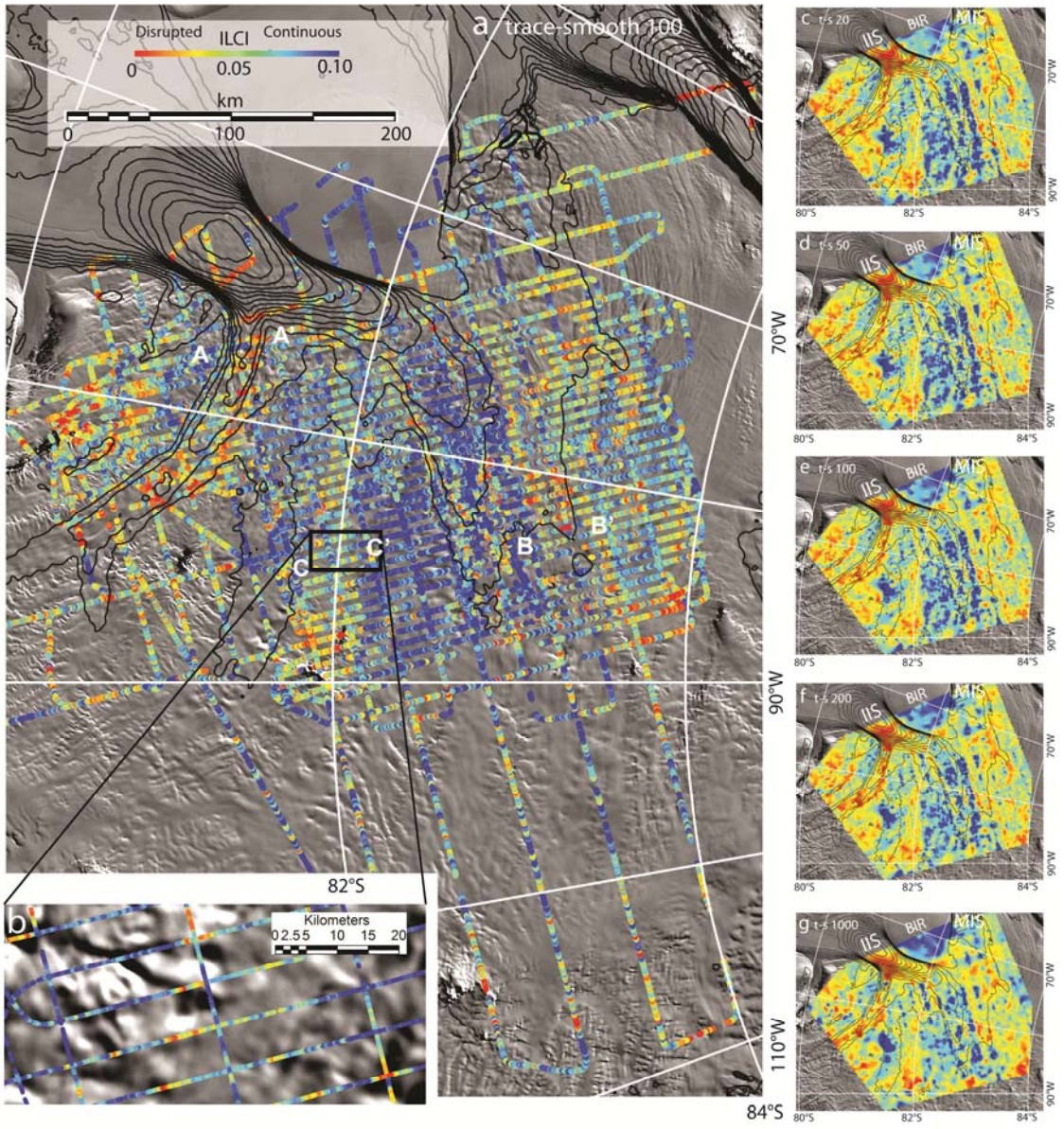

Figure S1. Results of ILCI applied over different moving-window lengths. In all panels results are superimposed over MOA imagery [*Haran et al.*, 2006] and black contours mark 25 m a^{-1} surface-ice-flow velocities from MEASURES [*Rignot et al.*, 2011]. (a) ILCI derived from 100-trace moving windows and plotted along flight tracks. Locations of profiles AA', BB' and CC' shown in Fig. 2 (b) to (d) are annotated. (b) Zoom of part of panel a, demonstrating consistency of ILCI change along parallel tracks, and also a qualitative apparent correspondence between ILCI change and a number of features in the surface imagery. (c) to (g): Gridded at 2.5 km^2 resolution using ArcGIS "Topo-to-Raster", ILCI results derived using 20-trace windows (c); 50-trace windows (d); 100-trace windows (e); 200-trace windows (f); and 1000-trace windows (g).

References

Bingham, R.G., M.J. Siegert, D.A. Young and D.D. Blankenship (2007) Organized flow from the South Pole to the Filchner-Ronne ice shelf: an assessment of balance velocities in interior East Antarctica using radio echo sounding data, J. Geophys. Res., 112, JF000556, doi: 10.1029/2006JF000556.

Karlsson, N.B., D.M. Rippin, R.G. Bingham, and D.G. Vaughan (2012) A 'continuity-index' for assessing ice-sheet dynamics from radar-sounded internal layers, Earth Planet. Sci. Lett., 335-336, 88-94, doi: 10.1016/j.epsl.2012.04.034.

Matsuoka, K. (2011) Pitfalls in radar diagnosis of ice-sheet bed conditions: Lessons from englacial attenuation models, Geophys. Res. Lett., 38, GL046205, doi: 10.1029/2010GL046205.

Rippin, D.M., M.J. Siegert, and J.L. Bamber (2003) The englacial stratigraphy of Wilkes Land, East Antarctica, as revealed by internal radio-echo sounding layering, and its relationship with balance velocities, Ann. Glaciol., 36, 189-196, doi: 10.3189/172756403781816356.

Siegert, M.J., A.J. Payne, and I. Joughin (2003) Spatial stability of Ice Stream D and its tributaries, West Antarctica, revealed by radio-echo sounding and interferometry, Ann. Glaciol., 37, 377–382, doi: 0.3189/172756403781816022.

Siegert, M., N. Ross, H. Corr, J. Kingslake, and R. Hindmarsh (2013) Late Holocene ice-flow reconfiguration in the Weddell Sea sector of West Antarctica, Quat. Sci. Rev., 78, 98-107, doi: 10.1016/j.quascirev.2013.08.003.

Sime, L.C., N.B. Karlsson, J.D. Paden, and S.P. Gogineni (2014) Isochronous information in a Greenland ice sheet radio echo sounding data set, Geophys. Res. Lett., 41, 1593-1599, doi: 10.1002/2013GL057928.

Vaughan, D. G., H. F. J. Corr, F. Ferraccioli, N. Frearson, A. O'Hare, D. Mach, J. W. Holt, D. D. Blankenship, D. A. Morse, and D. A. Young (2006) New boundary conditions for the West Antarctic Ice Sheet: subglacial topography beneath Pine Island Glacier, Geophys. Res. Lett., 33, L09501, doi: 10.1029/2005GL025588.

Woodward, J., and E.C. King (2009) Radar surveys of the Rutford Ice Stream onset zone, West Antarctica: indications of flow (in)stability, Ann. Glaciol., 50, 57-62, doi: 10.3189/172756409789097469.